RSC Advances

PAPER

View Article Online
View Journal | View Issue

Cite this: *RSC Adv.*, 2017, **7**, 20259

Experimental and *ab initio* studies of two UV nonlinear optical materials†

Juanjuan Lu,‡[ab] Guoqiang Shi,‡[ab] Hongping Wu,*[a] Ming Wen,[c] Dianwei Hou,[a] Zhihua Yang,[a] Fangfang Zhang*[a] and Shilie Pan*[a]

Received 18th February 2017
Accepted 24th March 2017

DOI: 10.1039/c7ra02027a

rsc.li/rsc-advances

Two new acentric polyborates, $Ba_3(OH)(B_9O_{16})[B(OH)_3]$ and $Ba_{2.16}Pb_{0.84}(OH)(B_9O_{16})[B(OH)_3]$ have been synthesized hydrothermally and their structures have been determined by single-crystal X-ray diffraction. Both crystals are isostructural and crystallize in the trigonal space group *P*31*c* (no. 159). Their structures feature a three-dimensional (3D) B_9O_{19} framework with 6-membered-ring tunnels, in which the Ba or Pb/Ba cations and $[B(OH)_3]$ groups reside. Powder second-harmonic-generation (SHG) measurements reveal that $Ba_3(OH)(B_9O_{16})[B(OH)_3]$ and $Ba_{2.16}Pb_{0.84}(OH)(B_9O_{16})[B(OH)_3]$ are type-**I** phase-matchable, with SHG responses of 1.1× and 1.2× KH_2PO_4, respectively. UV-Vis-NIR diffuse reflectance analysis indicates that $Ba_3(OH)(B_9O_{16})[B(OH)_3]$ and $Pb_{0.29}Ba_{2.71}(OH)(B_9O_{16})[B(OH)_3]$ have band gaps of 5.11 and 4.65 eV, respectively. In addition, first-principles calculations were employed to elucidate the origin of the NLO properties and the relationship of structure–properties.

Introduction

Nonlinear optical (NLO) materials have numerous important applications in semiconductor photolithography, laser micromachining, photochemical synthesis, and material processing due to their abilities to expand the frequency range of solid-state lasers from UV to IR.[1,2] Over the past decades, extensive efforts have been made to search for new NLO materials with excellent properties, including a large second harmonic generation (SHG) response and wide transparency window,[3] *etc.* To enhance the SHG response of the materials, "distortable" metal cations containing the d^0 or d^{10} transition metals (*e.g.*, Ti^{4+}, V^{5+}, Zn^{2+}, Cd^{2+}, *etc.*) and stereochemically active lone pair (SCALP) cations (Bi^{3+}, Pb^{2+}, Te^{4+}, *etc.*) are introduced into the crystal structures.[4–7] Unfortunately, the introduction of these cations always causes red shifts of the ultraviolet (UV) absorption edge. Compared with the d^0 or d^{10} transition metal, alkaline-earth metal cations have wide transmittances in UV region. In addition, borate is transparent in UV range as well. And it has a twice probability (in average) to be non-centrosymmetric than that of other inorganic compounds,[1a] which becomes a good candidate for NLO materials.

With this in minds, we combine the alkaline-earth metal cation with the borate system and successfully synthesize a new barium borate, $Ba_3(OH)(B_9O_{16})[B(OH)_3]$ (**I**), through the hydrothermal method. It has a large band gap of 5.11 eV and is type-**I** phase matchable with SHG responses of about 1.1× K_2HPO_4 (KDP). Through our investigation, barium atoms can be replaced by lead atoms to generate larger SHG response in many non-centrosymmetric structures.[8,9] For instance, $Pb_2Ba_3(BO_3)_3Cl$ exhibit a large SHG response 6× higher than its isomorphic compound $Ba_5(BO_3)_3Cl$. Thus, we tried to substitute lead for barium in compound **I** and obtained another new compound, $Ba_{2.16}Pb_{0.84}(OH)(B_9O_{16})[B(OH)_3]$ (**II**). To systematically study the substitution influence of the Pb cations on optical properties, we synthesize the polycrystalline samples of $Pb_3(OH)(B_9O_{16})[B(OH)_3]$ (**III**),[10] which is isomorphic with **I** and **II**. In this paper, we combine experimental characterization and theoretical calculations to study the optical properties among these three compounds. In addition, the thermal behavior and infrared (IR) spectra on these three compounds are also reported.

Experimental

Synthesis

All reagents were of analytical grade. Three compounds were synthesized under hydrothermal condition. The mixtures were mixed homogeneously and transferred to heat-sealed FEP Teflon pouches. The pouches were placed in 23 mL Teflon-lined stainless steel vessels and each vessel was added with about 8 mL

[a]*Key Laboratory of Functional Materials and Devices for Special Environments of CAS, Xinjiang Key Laboratory of Electronic Information Materials and Devices, Xinjiang Technical Institute of Physics & Chemistry of CAS, 40-1 South Beijing Road, Urumqi 830011, China. E-mail: slpan@ms.xjb.ac.cn; Fax: +86-991-3838957; Tel: +86-991-3674558*

[b]*University of Chinese Academy of Sciences, Beijing 100049, China*

[c]*School of Chemistry and Chemical Engineering, Harbin Institute of Technology, Harbin, Heilongjiang 150001, China*

† Electronic supplementary information (ESI) available. CCDC 1540435–1540437. For ESI and crystallographic data in CIF or other electronic format see DOI: 10.1039/c7ra02027a

‡ JJ and GQ contributed equally.

distilled water. Then the vessels were heated to 210 °C for 12 days and cooled to room temperature at a rate of 2 °C h^{-1}. The resulting colorless columnar crystals were obtained, washed with distilled water, and finally dried in air at ambient temperature.

Compound I. A mixture of $Ba(OH)_2 \cdot 8H_2O$ (0.210 g, 0.67 mmol), H_3BO_3 (0.227 g, 3.67 mmol) and 0.1 mL of anhydrous ethylenediamine was mixed homogeneously. The yield of the product was just about 10% based on $Ba(OH)_2 \cdot 8H_2O$. To increase the yield of compound **I**, we adjusted the proportion of raw material with a mixture of $Ba(NO_3)_2$ (0.090 g, 0.34 mmol), H_3BO_3 (0.106 g, 1.71 mmol), $Li(OH) \cdot H_2O$ (0.024 g, 0.57 mmol) and NH_4NO_3 (0.024 g, 0.15 mmol) in deionized water. Thus the yield of the product increases to 95% based on $Ba(NO_3)_2$.

Compound II. A mixture of $BaCO_3$ (0.099 g, 0.50 mmol), H_3BO_3 (0.247 g, 3.99 mmol), $Pb(CH_3COO)_2 \cdot 3H_2O$ (0.095 g, 0.25 mmol), PbF_2 (0.015 g, 0.06 mmol) and 0.2 mL NaOH solution (0.8 M) was mixed homogeneously. Colorless crystals of compound **II** were obtained in a yield of 85% based on $BaCO_3$.

Compound III. A mixture of PbO (0.186 g, 0.83 mmol), B_2O_3 (0.296 g, 4.25 mmol), and 0.2 mL of glacial acetic acid was mixed homogeneously. Colorless crystals of compound **III** were obtained in a yield of about 90% based on PbO.

Structural determination

Single crystals of compounds **I** and **II** were collected at room temperature on a Bruker SMART APEX **II** CCD diffractometer with graphite monochromatic Mo Kα radiation ($\lambda = 0.71073$ Å) at 296(2) K and integrated with the SAINT program.[11] The numerical absorption corrections were carried out using the SCALE program for area detector. All calculations were performed with programs from the SHELXTL crystallographic software package,[12] and all of the atoms were refined using full-matrix least-squares techniques with anisotropic thermal parameters and finally converged for $F_0^2 \geq 2\sigma(F_0^2)$. During the refinement, we found that in the structure of compound **I**, the Ba(1) atom has a large thermal factor and a large Q peak is around the Ba(1) atom. Refined with the split model, a Ba(1) site with 88.9% occupancy and a Ba(2) site with 11.1% occupancy converge with better *R* values and reasonable temperature factors. The structures were checked for missing symmetry elements by the program PLATON.[13] There was no higher symmetry to be found. Details of crystal parameters, data collection and structure refinements were shown in Table 1. The atomic coordinates, equivalent isotropic displacement coefficients and important bond lengths and angels were listed in Tables S1 and S2 in the ESI,† respectively. For comparison, the structure of compound **III** was reexamined and the data was also listed in Table 1.

Powder X-ray diffraction (XRD). Powder XRD patterns of polycrystalline sample of compounds **I**, **II** and **III** were obtained on a Bruker D2 PHASER diffractometer with Cu Kα radiation ($\lambda = 1.5418$ Å) at room temperature (Fig. S1 in the ESI†). The 2θ range was 10–70° with a step size of 0.02° and a fixed counting time of 1 s per step.

Infrared and UV-vis-NIR spectrum measurements. The IR spectrum was recorded with a Shimadzu IR Affinity-1 Fourier transform IR spectrometer in the 400–4000 cm^{-1} wave number range. The samples were mixed thoroughly with dried KBr (5 mg of each sample and 500 mg of KBr). UV-Vis-NIR diffuse reflectance spectrum was measured at room temperature on a Shimadzu SolidSpec-3700DUV spectrophotometer with a range from 190 to 2600 nm.

Thermal analysis

The thermal gravity-differential scanning calorimetric (TG-DSC) analyses were carried out on NETZSCH STA 449 °C instrument at a temperature range of 30–1000 °C with a heating rate of 10 °C min^{-1} under a constant flow of nitrogen gas.

Second-order NLO measurement

Powder SHG measurements were performed on a modified Kurtz-NLO system using a pulsed Nd:YAG laser (1064 nm, 10

Table 1 Crystal data and structure refinement results for compounds I, II and III

Empirical formula	**I**	**II**	**III**
Formula weight	844.15	902.78	1053.70
Crystal system	Trigonal	Trigonal	Trigonal
Space group, *Z*	*P*31*c*, 2	*P*31*c*, 2	*P*31*c*, 2
Unit cell dimensions	$a = 10.252(9)$ Å	$a = 10.218(8)$ Å	$a = 10.080(9)$ Å
	$c = 8.623(3)$ Å	$c = 8.587(1)$ Å	$c = 8.533(1)$ Å
Volume (Å^3)	785.0(3)	776.3(1)	751.0(1)
Density (calculated) (mg m^{-3})	3.571	3.910	4.642
Theta range for data collection (deg)	2.29 to 27.41	2.30 to 27.26	2.33 to 27.66
Limiting indices	$-13 \leq h \leq 11$, $-13 \leq k \leq 11$, $-9 \leq l \leq 11$	$-12 \leq h \leq 13$, $12 \leq k \leq 13$, $-9 \leq l \leq 11$	$-13 \leq h \leq 13$, $-11 \leq k \leq 13$, $-8 \leq l \leq 11$
Reflections collected/unique	4561/1139 [*R*(int) = 0.0539]	4331/1109 [*R*(int) = 0.0787]	4458/1044 [*R*(int) = 0.0440]
Completeness to theta	100.0%	100.0%	100.0%
Goodness-of-fit on F^2	1.150	1.071	1.004
Final *R* indices $[F_0^2 > 2\sigma(F_0^2)]^a$	$R_1 = 0.0457$, $wR_2 = 0.0919$	$R_1 = 0.0527$, $wR_2 = 0.1155$	$R_1 = 0.0239$, $wR_2 = 0.0403$
R indices (all data)[a]	$R_1 = 0.0489$, $wR_2 = 0.0931$	$R_1 = 0.0595$, $wR_2 = 0.1186$	$R_1 = 0.0264$, $wR_2 = 0.0412$
Extinction coefficient	0.0018(3)	0.0071(1)	0.0029(2)
Largest diff. peak and hole (e Å^{-3})	1.574 and −1.404	1.673 and −2.123	1.294 and −0.759

[a] $R_1 = \sum||F_0| - |F_c||/\sum|F_0|$ and $wR_2 = [\sum w(F_0^2 - F_c^2)^2/\sum wF_0^4]^{1/2}$ for $F_0^2 > 2\sigma(F_0^2)$.

kHz, 10 ns). A detailed description of the methodology has been published.[14] As the powder SHG efficiency has been shown to strongly depend on particle size. The crystals of three compounds were ground and sieved into distinct particle size ranges: <20, 20–38, 38–55, 55–88, 88–105, 105–150, and 150–200 μm, respectively. The microcrystalline samples of KDP served as the standard and were also sieved into the same particle size ranges.

Theoretical calculation details

The band structure of compounds **I** and **III** have been calculated by the first principles method. For compound **I**, we only think that the Ba(1) atoms are 100% occupancy used for the calculation, while for compound **II** calculations were not performed since the site disorder existed in the structure. The plane-wave pseudopotential method implemented in the CASTEP package[15] was used to calculate the electronic structure and NLO properties. We adopted GGA-PBE as the exchange correlation function and norm-conserving pseudopotential to treat electron–core interactions.[16,17] The kinetic energy cutoff was set as 800 and 870 eV for compounds **I** and **III**, respectively. The outmost electrons of H, B, and O, as well as Ba-$5s^2$ $5p^6$ $6s^2$ and Pb-$5s^2$ $5p^6$ $5d^{10}$ $6s^2$ $6p^2$, were considered to be valence electrons. The *k*-point was set as 2 × 2 × 2 for compounds **I** and **III**.

At a zero frequency, the SHG coefficients were calculated using the length-gauge formalism method derived by Aversa *et al.* and developed by Lin and Zhang *et al.*[18–20] The static second-order nonlinear coefficients can be ascribed to virtual-electron (VE) and virtual-hole (VH) processes,

$$x^{(2)}_{\alpha\beta\gamma} = x^{(2)}_{\alpha\beta\gamma}(\mathrm{VE}) + x^{(2)}_{\alpha\beta\gamma}(\mathrm{VH}). \quad (1)$$

Where $x^{(2)}_{\alpha\beta\gamma}(\mathrm{VE})$ and $x^{(2)}_{\alpha\beta\gamma}(\mathrm{VH})$ can be computed by the following eqn (2) and (3), respectively.

$$x^{(2)}_{\alpha\beta\gamma}(\mathrm{VE}) = \frac{e^3}{2\hbar^2 m^3}\sum_{\mathrm{vcc'}}\int\frac{d^3k}{4\pi^3}P(\alpha\beta\gamma)\mathrm{Im}\left[P_{\mathrm{cv}}{}^{\alpha}P_{\mathrm{cc'}}{}^{\beta}P_{\mathrm{c'v}}{}^{\gamma}\right] \times\left(\frac{1}{\omega_{\mathrm{cv}}{}^3\omega_{\mathrm{vc'}}{}^2}+\frac{2}{\omega_{\mathrm{vc}}{}^4\omega_{\mathrm{c'v}}}\right) \quad (2)$$

$$x^{(2)}_{\alpha\beta\gamma}(\mathrm{VH}) = \frac{e^3}{2\hbar^2 m^3}\sum_{\mathrm{vv'c}}\int\frac{d^3k}{4\pi^3}P(\alpha\beta\gamma)\mathrm{Im}\left[P_{\mathrm{vv'}}{}^{\alpha}P_{\mathrm{cv'}}{}^{\beta}P_{\mathrm{cv}}{}^{\gamma}\right] \times\left(\frac{1}{\omega_{\mathrm{cv}}{}^3\omega_{\mathrm{vc'}}{}^2}+\frac{2}{\omega_{\mathrm{vc}}{}^4\omega_{\mathrm{c'v}}}\right) \quad (3)$$

here, α, β, γ are Cartesian components, while v and v′ donate valence bands (VBs), c and c′ donate conduction bands (CBs). And then $P(\alpha\beta\gamma)$, $\hbar\omega_{ij}$ and $P_{ij}{}^{\alpha}$ refer to full permutation, the band energy difference and momentum matrix elements, respectively.

Results and discussion

Crystal structure

The compounds **I**, **II** and **III** are isostructural, hence, only the structure of compound **I** is discussed as the representative. Compound **I** crystallizes in a trigonal crystal system with an acentric space group of *P*31*c* (no. 159). In the asymmetric unit,

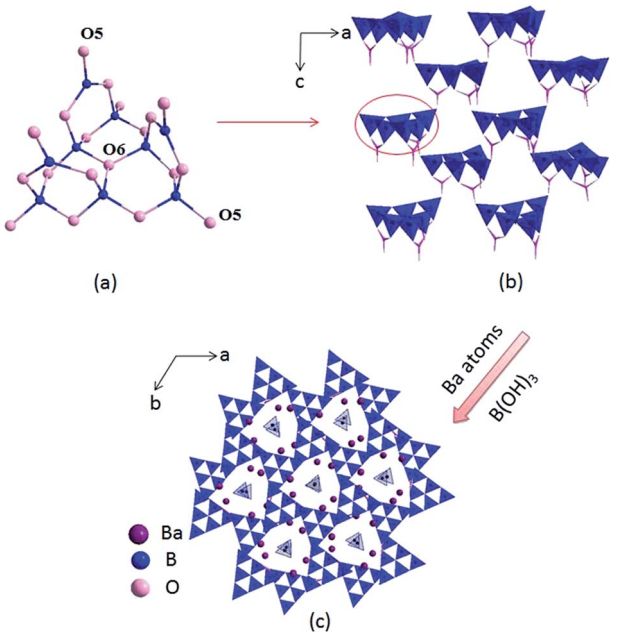

Fig. 1 Structure of compound I (the Ba–O bonds and H atoms are omitted for clarity).

the Ba, B and O atoms occupy one, four and eight crystallographically unique positions, respectively (Table S1 in the ESI†). The B atoms are bonded to three or four O atoms to form two kinds of coordination models BO_3 triangles and BO_4 tetrahedra. Six BO_4 tetrahedra connected with three BO_3 triangles to construct B_9O_{19} group (Fig. 1a), which further connected by sharing oxygen atoms to build a 3D framework with tunnels along *c* axis (Fig. 1b), where the Ba atoms and $B(OH)_3$ reside in (Fig. 1c).

In the structure of compound **I**, the Ba atoms are connected with nine O atoms to form the $Ba(1)O_9$ polyhedra, with the Ba–O bond lengths ranging in 2.496(3)–3.192(1) Å (average = 2.811(0) Å). Three $Ba(1)O_9$ polyhedra connect with each other by sharing edges to form the 3D Ba–O framework (Fig. S2 in the ESI†). The B–O distances vary from 1.347(1)–1.441(1) Å (average = 1.376(5) Å) in the BO_3 triangles and 1.442(1)–1.534(1) Å (average = 1.472(3) Å) in the BO_4 tetrahedra, respectively, which are also similar to reported values in other borates, such as $Ba_4B_{11}O_{20}F$,[5d] $M_2Ca_3B_{16}O_{28}$ (M = Rb, Cs)[21] and $Sr_4B_{10}O_{18}(OH)_2\cdot 2H_2O$.[22] In addition, the bond valences of the Ba, Pb, B and O atoms have been calculated according to the Brown parameters for compounds **I**, **II** and **III** and are listed in Table S1 in the ESI,† which are in agreement with their ideal oxidation state (Ba, +2; Pb, +2; B, +3; O, −2).

Compounds **I**, **II** and **III** are isostructural and their fundamental structure units are all B_9O_{19} group, which further connected with each other to build the 3D framework. While the coordination of the cations are not the same. In compound **II**, one site is occupied by constitutionally disordered Pb and Ba atoms, which is different from the total occupation of atoms on each site for compound **III**. In addition, in compounds **I** and **II**, the Ba atoms and Pb/Ba atoms

Table 2 Assignments of the infrared absorption peaks for compounds I, II and III

Mode description	**I** (cm^{-1})	**II** (cm^{-1})	**III** (cm^{-1})
Characteristic peak of OH	3007	3455	3441
Asymmetric stretching of B_3–O	1433, 1284	1424, 1318, 1267	1432, 1347, 1259
Asymmetric stretching of B_4–O	1130, 1060	1122, 1056	1120, 1056
Symmetric stretching of B_3–O	925	939	950
Symmetric stretching of B_4–O	803	815	810
Out-of-plane bending of B_3–O	756, 658, 614	747, 664	743, 663, 601
Bending of B_4–O and B_3–O	523	510	518

are both located in nine coordination environments to form the $Ba(1)O_9$ and Ba/PbO_9 polyhedra, respectively. While in compound **III**, the Pb atoms are located in four coordination environments to form the PbO_4 tetrahedra. Then three PbO_4 tetrahedra are linked by sharing O_7 atoms to form isolated Pb_3O_{10} unit (Fig. S1c†).

Thermal analysis

The TG-DSC curves of three compounds are shown (Fig. S3†). Hydroxyl groups exist in three compounds, but at a relatively high temperature, it will be removed in the form of water molecule. Evident weight loss has been observed for compounds **I**, **II** and **III** in the temperature range 400–700, 400–600 and 200–300 °C, respectively. For compound **I**, the weight loss is 7.3%, which is due to the release of 3.5 molecules H_2O per formula unit (calculated value 7.5%). For compound **II**, the weight loss of 3.9% is due to the releases of the two molecules H_2O (calculated 4.0%). While for compound **III**, the weight loss is 1.8% due to the release of one molecule H_2O (calculated 1.7%).

IR spectrum

The IR spectra of compounds **I**, **II** and **III** are shown in Fig. S4.† Accordingly the absorption peaks are listed in Table 2. The spectra are similar on these three compounds. We can see that the absorption peaks locate at 3000–3450 cm^{-1} assigning to the vibrations of the OH groups. The strong absorption peaks between 1259 and 1433 cm^{-1} can be attributed to the asymmetric stretching of the BO_3 groups, whereas the absorption peaks at about 925–950 cm^{-1} can be attributed to the symmetric stretching of the BO_3 groups. The peaks located at ~1120 and ~810 cm^{-1} are the asymmetric and symmetric stretching of the BO_4 groups, respectively. The bending vibrations of the BO_3 and BO_4 groups can be observed in the range 510–756 cm^{-1}. The results show that the BO_3 and BO_4 groups exist in the three compounds.[23,24]

UV-Vis-NIR diffuse reflectance spectroscopy

The optical diffuse reflectance spectra of compounds **I**, **II** and **III** in the region 190–2600 nm were measured (Fig. S5†). Reflectance spectra were converted to absorbance using the function, $F(R) = (1 - R)^2/2R$, where R is the reflectance and $F(R)$ is the Kubelka–Munk remission function.[25,26] It is obtained that the experimental energy gaps of compounds **I**, **II** and **III** are 5.11, 4.65 and 4.58 eV, respectively (Fig. 2). Obviously, there is a red shift of the absorption edges from compound **I** to **III** due to the substitution of Pb for Ba atom.

The first principle calculation results show that compounds **I** and **III** are indirect band gap compounds with calculated band gap 4.76 eV for compound **I** and 4.16 eV for compound **III** (Fig. 3). The calculated band gaps are smaller than the experimental ones, which is mainly caused by the inaccuracy of the exchange correlation energy.[27,28]

To better understand the relationship between electronic structures and optical properties, the density of states (DOS) of compounds **I** and **III** were compared and shown in Fig. 4. At the valence band, the two compounds have similar electronic structures: the inner valence orbitals for the constituent ions (*i.e.*, O-2s orbitals, B-sp mixed orbitals, Ba-4s orbitals, and H-s orbitals), respectively. The valence bands from −10 to 0 eV for both compounds are mainly composed of the O-2p orbitals, B-2p orbitals, Ba-4p orbitals and H-s orbitals, respectively, and the

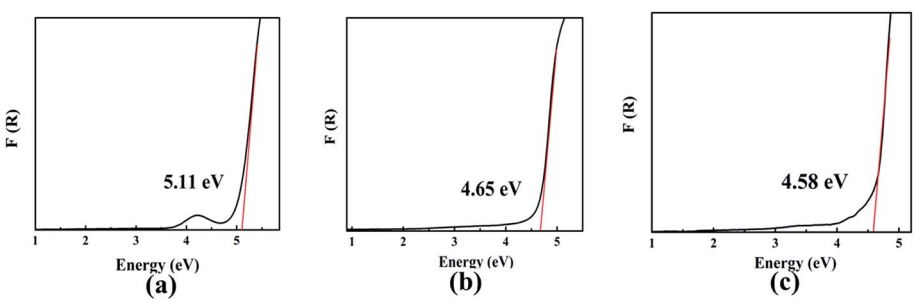

Fig. 2 The optical absorption spectra of compounds I (a), II (b) and III (c).

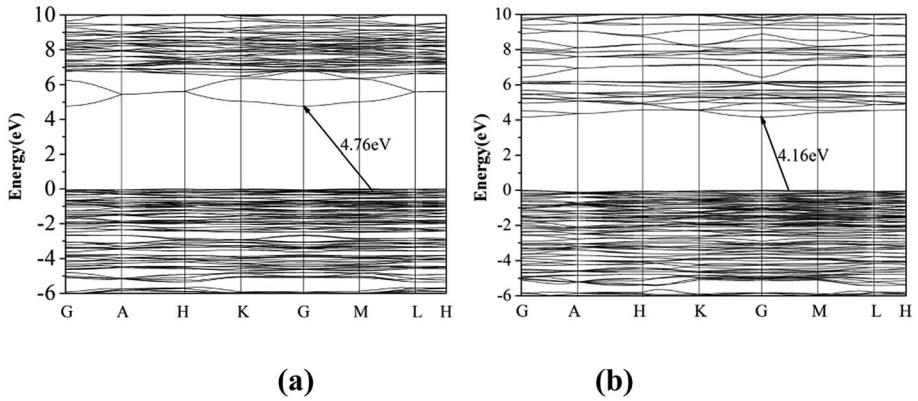

Fig. 3 The band gap of compounds I (a) and III (b).

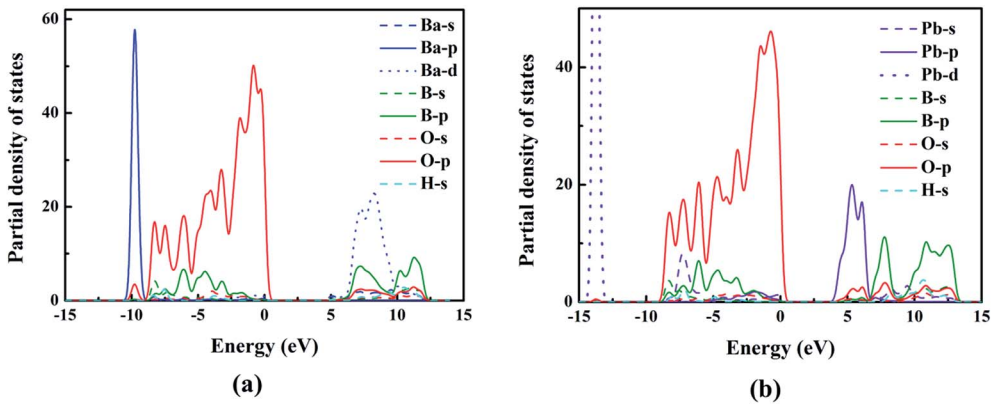

Fig. 4 The PDOS of compounds I (a) and III (b).

O-2p orbitals have dominant contribution to the maximum of the valence bands. The conduction bands are mainly composed of B-2p orbitals, O-2p orbitals and Ba-5d for compound **I**, and B-2p orbitals, O-2p orbitals and Pb-6p for compound **III**. We can see that Pb-6p orbitals of compound **III** locate nearer to the Fermi level than Ba-5d orbitals of compound **I**, which cause the small red shift of the band gaps from compound **I** to compound **III**.

Second-harmonic generation effects

We have also investigated their SHG responses since the title compounds belong to a NCS space group ($P31c$). Compounds **I**, **II** and **III** exhibit a SHG response of 1.1, 1.2 and 2.7 times that of KDP, respectively (Fig. 5), which indicates that the Pb substitution can enhance the SHG response in the three compounds. In addition, compounds **I**, **II** and **III** are all type-**I** phase matchable because the second-harmonic intensities increase with the increase of particle size and go to saturation values.

To visualize the SHG response of electronic states of compounds **I** and **III**, the SHG-density method[29] was used to analyze the relationship between optical properties and electronic states. Since the VE and VH have the important effect on the SHG coefficient, both processes were analyzed. For compounds **I** and **III**, it crystallizes $3m$ point group, there are three non-zero NLO coefficients. For d_{22} of compound **I**, the contribution from the VE is 64.1% and VH is 35.9% (Fig. 6). In the occupied states, the O(8)-2p orbitals are dominant in both VE and VH processes. While in unoccupied states, the O(6)-2p

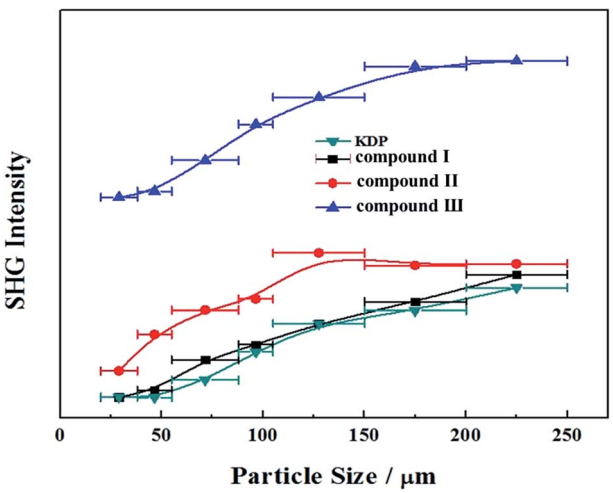

Fig. 5 Powder SHG of compounds I, II and III at 1064 nm. Curves are drawn to guide the eye and are not a fit to the data.

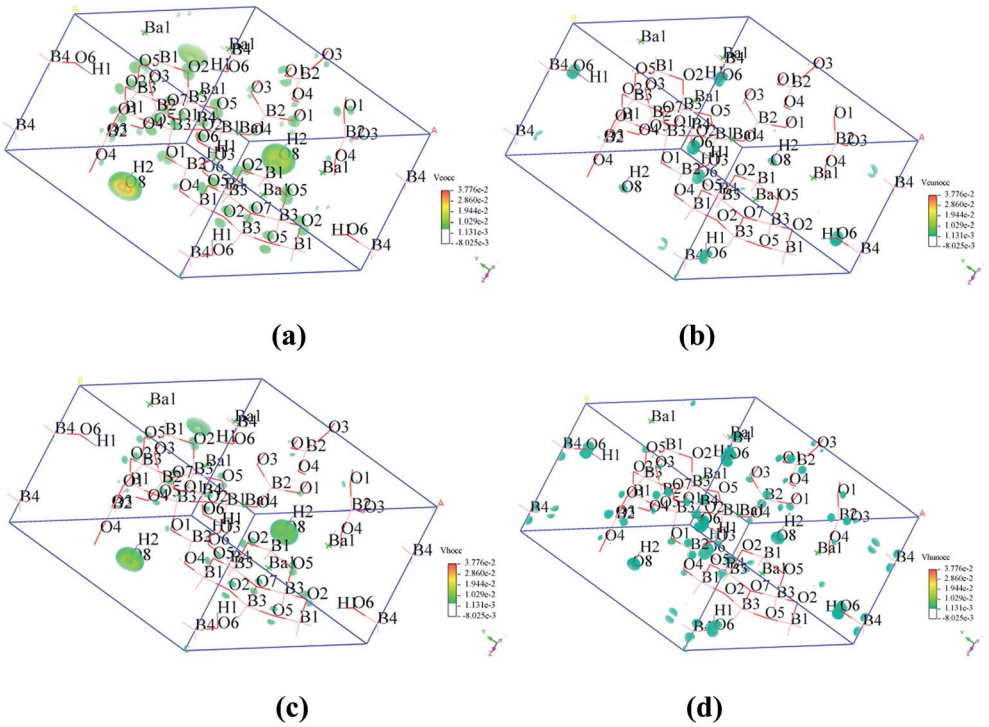

Fig. 6 SHG-weighted electron densities of the occupied and unoccupied orbitals in the VE and VH processes of compound I. (a) Occupied orbitals of VE process; (b) unoccupied orbitals of VE process; (c) occupied orbitals of VH process; (d) unoccupied orbitals of VH process.

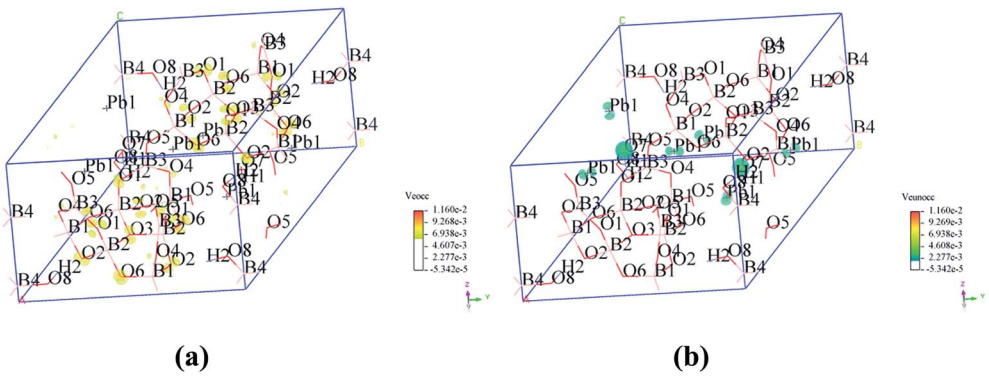

Fig. 7 SHG-weighted electron densities of the occupied and unoccupied orbitals in the VE processes of compound III. (a) Occupied orbitals of VE process; (b) unoccupied orbitals of VE process.

and O(8)-2p orbitals are main contributors in the VE process. The B(2)-2p and B(4)-2p orbitals play major roles in the VH process. Thus, the B–O groups have the important contribution on the SHG. For compound **III**, VE processes are the main contributions to the d_{22} SHG coefficients (Fig. 7). The analysis shows that the main contributions are BO_3 groups and lead cations with stereochemically active lone pair.

Conclusion

Combining alkaline earth metal with borate, new compounds, $Ba_3(OH)(B_9O_{16})[B(OH)_3]$ and $Pb_{0.29}Ba_{2.71}(OH)(B_9O_{16})[B(OH)_3]$ have been synthesized by the hydrothermal method for the first time. Their structures feature a three-dimensional (3D) B_9O_{19} framework with tunnels along *c*-direction, in which the Ba or Pb/Ba cations and $[B(OH)_3]$ groups dwell. $Ba_3(OH)(B_9O_{16})[B(OH)_3]$, $Pb_{0.29}Ba_{2.71}(OH)(B_9O_{16})[B(OH)_3]$ and $Pb_3(OH)(B_9O_{16})[B(OH)_3]$ are type-**I** phase-matchable, with SHG responses 1.1, 1.2 and 2.7× KDP, respectively. The band gap of $Ba_3(OH)(B_9O_{16})[B(OH)_3]$ (5.11 eV) is larger than that of $Pb_3(OH)(B_9O_{16})[B(OH)_3]$ (4.65 eV). First-principle calculations reveal that the bottom of conduction band of $Ba_3(OH)(B_9O_{16})[B(OH)_3]$ is dominated by Ba-5d orbital, while, in $Pb_3(OH)(B_9O_{16})[B(OH)_3]$, the bottom of conduction band is dominated by Pb-6p orbital. The SHG response density shows that the B–O groups have the important contribution to SHG response in $Ba_3(OH)(B_9O_{16})[B(OH)_3]$. While the BO_3 groups and

lead cations with stereochemically active lone pair have main contribution in $Pb_3(OH)(B_9O_{16})[B(OH)_3]$.

Acknowledgements

This work is supported by the Western Light Foundation of CAS (Grant 2016-QNXZ-A-2), 973 Program of China (Grant No. 2014CB648400), the National Natural Science Foundation of China (Grant No. U1303392, 51425206), the Youth Innovation Promotion Association CAS (Grant 2015353).

References

1 (*a*) P. Becker, *Adv. Mater.*, 1998, **10**, 979; (*b*) C. T. Chen, B. C. Wu, A. D. Jiang and G. M. You, *Sci. Sin., Ser. B*, 1985, **28**, 235; (*c*) M. E. Hagerman and K. R. Poeppelmeier, *Chem. Mater.*, 1995, **7**, 602.

2 (*a*) P. G. Schunemann, P. A. Budni and K. L. Schepler, *Mater. Res. Bull.*, 1998, **23**, 45; (*b*) D. F. Eaton, *Science*, 1991, **253**, 281.

3 (*a*) Y. C. Wu, T. Sasaki, S. Nakai, A. Yokotani, H. Tang and C. T. Chen, *Appl. Phys. Lett.*, 1993, **62**, 2614; (*b*) Y. Mori, I. Kuroda, S. Nakajima, T. Sasaki and S. Nakai, *Appl. Phys. Lett.*, 1995, **67**, 1818; (*c*) L. Cheng, *J. Cryst. Growth*, 1991, **110**, 697; (*d*) A. O. Okorogu, S. B. Mirov, W. Lee, D. I. Crouthamel, N. Jenkins, A. Y. Dergachev, K. L. Vodopyanov and V. V. Badikov, *Opt. Commun.*, 1998, **155**, 307; (*e*) G. D. Boyd, T. J. Bridges and C. K. N. Patel, *Appl. Phys. Lett.*, 1972, **21**, 553; (*f*) H. S. Ra, K. M. Ok and P. S. Halasyamani, *J. Am. Chem. Soc.*, 2003, **125**, 7764.

4 (*a*) G. H. Zhou, Z. J. Ma, K. C. Wu and N. Ye, *J. Mater. Chem.*, 2012, **22**, 19911; (*b*) G. H. Zou, G. Nam, H. G. Kim, H. Jo, T. S. You and K. M. Ok, *RSC Adv.*, 2015, **5**, 84754; (*c*) H. W. Huang, J. Y. Yao, Z. S. Lin, X. Y. Wang, R. He, W. J. Yao, N. X. Zhai and C. T. Chen, *Angew. Chem.*, 2011, **123**, 10456; (*d*) Y. Z. Huang, L. M. Wu, X. T. Wu, L. H. Li, L. Chen and Y. F. Zhang, *J. Am. Chem. Soc.*, 2010, **132**, 12788; (*e*) S. C. Wang, N. Ye, W. Li and D. Zhao, *J. Am. Chem. Soc.*, 2010, **132**, 8779.

5 (*a*) G. H. Zou, C. S. Lin, H. Jo, G. Nam, T. S. You and K. M. Ok, *Angew. Chem., Int. Ed.*, 2016, **128**, 12257; (*b*) K. Wu, Z. H. Yang and S. L. Pan, *Angew. Chem., Int. Ed.*, 2016, **55**, 6713; (*c*) J. L. Song, C. L. Hu, X. Xu, F. Kong and J. G. Mao, *Angew. Chem., Int. Ed.*, 2015, **54**, 3679; (*d*) Y. Wang and S. L. Pan, *Coord. Chem. Rev.*, 2016, **323**, 15; (*e*) H. P. Wu, H. W. Yu, Z. H. Yang, X. L. Hou, S. L. Pan, X. Su, K. R. Poeppelmeier and J. M. Rondinelli, *J. Am. Chem. Soc.*, 2013, **135**, 4215.

6 (*a*) W. L. Zhang, W. D. Cheng, H. Zhang, L. Geng, C. S. Lin and Z. Z. He, *J. Am. Chem. Soc.*, 2010, **132**, 1508; (*b*) H. W. Yu, S. L. Pan, H. P. Wu, W. W. Zhao, F. F. Zhang, H. Y. Li and Z. H. Yang, *J. Mater. Chem.*, 2012, **22**, 2105; (*c*) L. Wang, S. L. Pan, L. Chang, J. Hu and H. Yu, *Inorg. Chem.*, 2012, **51**, 1852.

7 (*a*) M. Wen, X. Su, H. P. Wu, J. J. Lu, Z. H. Yang and S. L. Pan, *J. Phys. Chem. C*, 2016, **120**, 6190; (*b*) F. F. Zhang, F. Y. Zhang, B. H. Lei, Z. H. Yang and S. L. Pan, *J. Phys. Chem. C*, 2016, **120**, 12757; (*c*) M. Wen, Z. P. Lian, H. P. Wu, X. Su, Q. F. Yan, J. J. Lu, Z. H. Yang and S. L. Pan, *RSC Adv.*, 2015, **5**, 53448.

8 (*a*) X. Y. Dong, Q. Jing, Y. J. Shi, Z. H. Yang, S. L. Pan, K. R. Poeppelmeier, J. Young and J. M. Rondinelli, *J. Am. Chem. Soc.*, 2015, **137**, 9417; (*b*) H. Y. Li, H. P. Wu, X. Su, H. W. Yu, S. L. Pan, Z. H. Yang, Y. Lu, J. Han and K. R. Poeppelmeier, *J. Mater. Chem. C*, 2014, **2**, 1704.

9 Z. H. Chen, S. L. Pan, Z. H. Yang, X. Y. Dong, X. Su and Y. Yang, *J. Mater. Sci.*, 2013, **48**, 2590.

10 E. L. Belokoneva, S. Y. Stefanovich, T. A. Borisova and O. V. Dimitrova, *Russ. J. Inorg. Chem.*, 2001, **46**, 1621.

11 *SAINT, Version 7.60A*, Bruker Analytical X-ray instruments, Inc., Madison, WI, 2008.

12 G. M. Sheldrick, *SHELXTL-97 Sheldrick: Program for Crystal Structure Refinement*, University of Gottingen, Germany, 1997.

13 A. L. Spek, *J. Appl. Crystallogr.*, 2003, **36**, 7.

14 L. Bohaty, *Z. Kristallogr. Cryst. Mater.*, 1983, **164**, 279.

15 S. J. Clark, M. D. Segall, C. J. Pickard, P. J. Hasnip, M. J. Probert, K. Rrfson and M. C. Payne, *Z. Kristallogr.*, 2005, **220**, 567.

16 J. P. Perdew, K. Burke and M. Ernzerhof, *Phys. Rev. Lett.*, 1996, **77**, 3865.

17 I. Varga, J. Pipek and B. Vasvári, *Phys. Rev. B: Condens. Matter Mater. Phys.*, 1992, **46**, 4978.

18 C. Aversa and J. E. Sipe, *Phys. Rev. B: Condens. Matter Mater. Phys.*, 1995, **52**, 14636.

19 J. Lin, M. H. Lee, Z. P. Liu, C. Chen and C. J. Pickard, *Phys. Rev. B: Condens. Matter Mater. Phys.*, 1999, **60**, 13380.

20 B. B. Zhang, Z. H. Yang, Y. Yang, M.-H. Lee, S. L. Pan, Q. Jing and X. Su, *J. Mater. Chem. C*, 2014, **2**, 4133.

21 X. Y. Zhang, D. N. Li, H. P. Wu, Z. H. Yang and S. L. Pan, *RSC Adv.*, 2016, **6**, 14205.

22 F. Y. Zhang, Q. Jing, F. F. Zhang, S. L. Pan, Z. H. Yang, J. Han, M. Zhang and S. J. Han, *J. Mater. Chem. C*, 2014, **2**, 667.

23 (*a*) X. F. Wang, F. F. Zhang, B. H. Lei, Z. H. Yang and S. L. Pan, *RSC Adv.*, 2016, **6**, 100849; (*b*) G. Q. Shi, F. F. Zhang, B. B. Zhang, D. W. Hou, X. L. Chen, Z. H. Yang and S. L. Pan, *Inorg. Chem.*, 2017, **56**, 344; (*c*) H. P. Wu, X. Su, S. J. Han, Z. H. Yang and S. L. Pan, *Inorg. Chem.*, 2016, **55**, 4806.

24 (*a*) Y. Yang, X. Su, S. L. Pan, M. Zhang, Y. Wang, J. Han and Z. H. Yang, *CrystEngComm*, 2014, **16**, 1978; (*b*) E. L. Belokoneva, E. A. Ruchkina and O. V. Dimitrova, *Russ. J. Inorg. Chem.*, 2001, **46**, 20.

25 P. Kubelka and F. Munk, *Z. Tech. Phys.*, 1931, **12**, 593.

26 J. Tauc, *Mater. Res. Bull.*, 1970, **5**, 721.

27 M. K. Y. Chan and G. Ceder, *Phys. Rev. Lett.*, 2010, **105**, 196403.

28 J. P. Perdew and M. Levy, *Phys. Rev. Lett.*, 1983, **51**, 188.

29 C. H. Lo, Master Degree Thesis, Tamkang University, 2005.